Compensation of Gravity-Induced Errors on a Hexapod-Type Parallel Kinematic Machine Tool*

Soichi IBARAKI**, Toshihiro OKUDA**,
Yoshiaki KAKINO**, Masao NAKAGAWA***,
Tetsuya MATSUSHITA*** and Tomoharu ANDO***

This paper presents a methodology to compensate contouring errors introduced by the gravity on a Hexapod-type parallel kinematic machine tool with the Stewart platform. Unlike conventional serial kinematic feed drives, the gravity imposes a critical effect on the positioning accuracy of a parallel kinematic feed drive, and its effect significantly varies depending on the position and the orientation of the spindle. We first present a kinematic model to predict the elastic deformation of struts caused by the gravity. The positioning error at the tool tip is given as the superposition of the deformation of each strut. It is experimentally verified for a commercial parallel kinematic machine tool that the machine's contouring error is significantly reduced by compensating gravity-induced errors on a reference trajectory.

Key Words: Machine Tool, Motion Control, Parallel Kinematic Machine Tool, Gravity-Induced Errors, Contouring Accuracy

1. Introduction

Most of machine tools in today's market are driven by feed drives that are aligned serially. For example, a 5-axis machine typically has three linear axes aligned orthogonal to each other, and two rotary axes aligned parallel to linear axes. As a counterpart to such a mechanism, which is referred to as a serial kinematic machine in this paper, parallel kinematic feed drives have recently attracted increasing attention for application in a machine tool due to their potentials in high-speed and high-accuracy 6-DOF (degrees of freedom) positioning. For example, compared to serial kinematic machines, the moving mass in parallel kinematic feed drives can be smaller since they do not need guideways, which is an advantage for high-speed and high-acceleration positioning. In parallel kinematic feed drives, an error in each axis does not impose an accumulating effect on the machine's positioning accuracy, which is a potential advantage for high-accuracy motion control[1].

The first prototype of Hexapod-type parallel kinematic machine tools was introduced to the public in 1994 by Ingersoll and Giddings & Lewis. A comprehensive review on the development of the parallel kinematics for machine tools can be found in Ref. (1). Although more than ten years have passed since the first commercial parallel kinematic machine tool was introduced, they are not widely accepted in today's industry. Despite many conceptual advantages of parallel kinematic feed drives, there are critical and inherent issues with their application in a machine tool[2]. One such issue is the stiffness; in a parallel kinematic machine tool, a spindle unit is supported and driven by struts only. It typically exhibits lower stiffness against an external force, compared to conventional feed drives with a guideway that introduces higher friction.

Furthermore, for parallel kinematic feed drives, the position and the orientation of the tool can be only

* Received 15th October, 2003 (No. 03-4130)
** Department of Precision Engineering, Kyoto University, Yoshida-honmachi, Sakyo-ku, Kyoto 606-8501, Japan. E-mail: ibaraki@prec.kyoto-u.ac.jp
*** Okuma Corporation, Oguchi-cho, Aichi 480-0193, Japan

indirectly estimated from the angular position of servo motors, unlike in the case of conventional serial kinematic feed drives. Therefore, for their high-accuracy motion control, the calibration of various kinematic parameters, such as the reference length of struts and the location of base joints, is a critical issue. There have been many research works found in the literature on the calibration of kinematic parameters to improve the positioning accuracy of a parallel kinematic machine tool. For example, Weck and Staimer[2] used a redundant leg, and Soons[3] used a laser interferometer to measure the machine's contouring error at the tool tip in order to indirectly identify kinematic errors. The kinematic calibration method based on circular tests[4] has been widely accepted by the industry due to the simplicity of its measurement procedure (Ota et al.[5], Oiwa et al.[6], and Takeda et al.[7]). In our previous work[8], we also presented a calibration methodology based on circular tests considering the gravity effect. By applying the kinematic calibration, the circularity error was reduced to as small as 5 μm, when the spindle was located near the center of the workspace. However, when the spindle was near an edge of the workspace and was tilted, or when its tilt angle was large even though it was located near the center of the workspace, the circularity error became as large as 200 μm at maximum. This error is commonly observed in any types of parallel kinematic machine tools, and it cannot be completely compensated even when kinematic parameters are accurately calibrated.

This error is attributable to the elastic deformation of struts caused by the gravity. On a parallel kinematic feed drive, the effect of gravity on the machine's positioning accuracy significantly varies depending on the position and the orientation of the spindle. It becomes particularly large when the spindle is located near a singular point of parallel kinematics. The motion accuracy of conventional serial kinematic machine tools also degrades near an edge of the workspace or when the tilt angle is large. In the case of parallel kinematic machines, this is more critical since it does not have a guideway to support against gravity. If the effect of the gravity can be accurately predicted a priori and compensated, the motion accuracy can be significantly improved over the entire workspace, assuming that the error in the calibration of kinematic parameters is sufficiently small. Weck et al.[2] presented a compensation method of gravity-induced positioning errors based on a simple kinematic model considering only the axial deformation of struts. Ota et al.[9] also presented a compensation scheme based on a more complex model considering the elastic deformation of joints as well.

This paper first presents a simulation model to predict gravity-induced contouring errors on a Hexapod-type parallel kinematic machine tool. The proposed model considers the elastic deformation of each strut due to the gravity imposed on a platform plate, a strut, a joint, and a servo motor, as well as the rotational friction in a base joint. The accuracy of the proposed model is validated by comparing servo motor loads for each strut and their estimate by the proposed model. The proposed model is simpler than the one presented by Ota et al.[9], and the parameters included in the model is easier to identify by simple identification tests. When its parameters are properly identified, it is experimentally verified that the model exhibits an excellent prediction performance.

It should be emphasized that the motion error due to the miscalibration of kinematic parameters must be minimized in order for an effective gravity compensation. When the kinematic parameters are calibrated in a sufficient accuracy, the motion error due to the gravity can be accurately predicted by using the simulation model. By compensating the predicted positioning error on a reference trajectory, the machine's contouring accuracy can be significantly improved over a large portion of the entire workspace.

The remainder of this paper is organized as follows. The following section briefly reviews the configuration and the kinematics of a Hexapod-type parallel kinematic machine tool with the Stewart platform. Simulation and compensation schemes of gravity-induced motion errors on Hexapod-type parallel kinematic machine tools are presented in section 3. Section 4 presents the experimental validation of the proposed compensation scheme. Section 5 gives the conclusion of this paper.

2. Configuration and Kinematics of a Hexapod-Type Parallel Kinematic Machine Tool

2.1 Configuration of a Hexapod-type parallel kinematic machine tool

This paper presents a compensation scheme of gravity-induced errors on a parallel kinematic feed drive of the Stewart platform[10] depicted in Fig. 1. It has six telescoping struts, each of which is connected to a base plate by a 2-DOF joint. The other end of a strut is connected by a 3-DOF joint to a platform plate, where a spindle is installed.

Figure 2 shows a schematic view of COSMO CENTER PM-600 developed by Okuma Corp., a commercial Hexapod-type parallel kinematic machining center with the Stewart platform, which is used as an experimental machine throughout our study. Table 1 shows its major specifications. Each strut is driven by a built-in servo motor via a ball screw. The "length"

Table 1 Major specifications of PM-600

Workspace, mm	ϕ600 (XY) ×400 (Z) (420 × 420 × 400)
Maximum tilt angle, deg	±25
Maximum rapid traverse speed, m/min	100
Maximum acceleration, m/s^2	14.7
Spindle speed, min^{-1}	12,000/30,000
Spindle power, kW	6

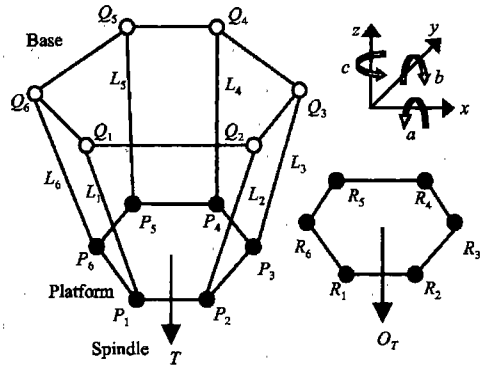

Fig. 1 Stewart platform

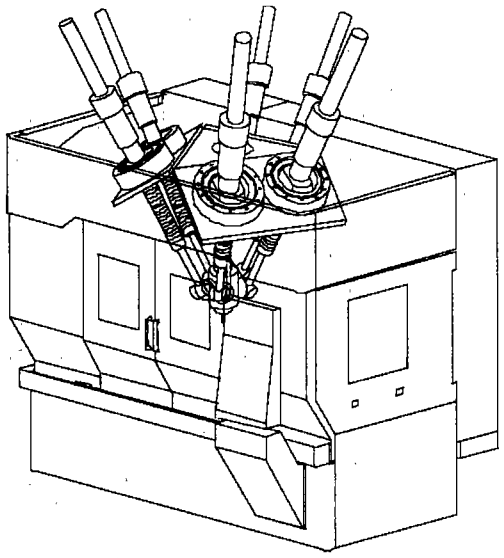

Fig. 2 A Hexapod-type parallel mechanism machine tool, COSMO CENTER PM600 by Okuma Corp.

of each strut is indirectly measured by a rotary encoder installed in a servo motor. In this paper, six joints on the platform plate are referred to as platform joints, while those on the base plate are referred to as base joints.

2.2 Inverse and forward kinematics of the Stewart platform

In Fig. 1, $\boldsymbol{T}=[X, Y, Z, A, B, C]$ represents the position and the orientation of the spindle tip (tool tip). When $\boldsymbol{T}$ is given, the problem to calculate the length of each strut, $\boldsymbol{L}=[L_1, \cdots, L_6]$, is called the inverse kinematic problem. It is denoted as:

$$\boldsymbol{L}=\mathcal{F}(\boldsymbol{T}) \quad (1)$$

where $\mathcal{F}$ represents the inverse kinematic function of the Stewart platform. Note that $\mathcal{F}$ is a function of the location of platform joints, $\boldsymbol{P}_j \in \boldsymbol{R}^3$ $(j=1-6)$, and the location of base joints, $\boldsymbol{Q}_j \in \boldsymbol{R}^3$ $(j=1-6)$. The inverse kinematic problem for the Stewart platform can be algebraically solved[8]. On the other hand, a problem to calculate $\boldsymbol{T}$ for the given $\boldsymbol{L}$ is referred to as the forward kinematic problem:

$$\boldsymbol{T}=\mathcal{F}^{-1}(\boldsymbol{L}) \quad (2)$$

The forward kinematic problem of the Stewart platform cannot be algebraically solved. In our simulator, the Newton-Raphson method is employed to numerically solve it.

3. Estimation and Compensation of Gravity-Induced Positioning Errors

3.1 An estimation model of gravity-induced positioning errors

This section presents a simulation model to predict the axial force imposed on each strut by gravity. The positioning error at the tool tip is estimated as the superposition of the elastic axial deformation of each strut, which is proportional to the axial force.

In our previous study[11], we presented an FEM analysis on the experimental machine to show that the positioning error in the XY plane due to the gravity is mostly caused by the axial deformation of struts. The contribution of the bending of struts on the contouring error in circular tests is much less than that of the axial deformation. Therefore, we only consider the axial deformation of each strut and ignore its bending to estimate the positioning error at the tool tip. Although we have not experimentally validated this analysis, we assume that this simplification is reasonable, since the proposed model without the consideration of the bending of struts showed good estimation performance, as will be shown later. The simulation model proposed in this paper assumes that the force acting on each strut is attributable only to: 1) the gravity and 2) the friction on a ball screw and a joint. Sections 3.1.1, 3.1.2 respectively discuss the simulation of each component.

3.1.1 Gravity model for each strut First, for convenience of notation, we define the following function, $\Gamma_{l,B}(x)$: $\boldsymbol{R}^6 \rightarrow \boldsymbol{R}^6$ by:

$$\Gamma_{l,B}(x)=\begin{bmatrix} \sum_{j=1}^{6}(x_j \boldsymbol{l}_j) \\ \sum_{j=1}^{6}(\boldsymbol{B}_j \times x_j \boldsymbol{l}_j) \end{bmatrix} \quad (3)$$

where $\boldsymbol{l}_j \in \boldsymbol{R}^3$ $(j=1-6)$ represents a unit vector in the direction of the j-th strut. $\boldsymbol{B}_j \in \boldsymbol{R}^3$ $(j=1-6)$ represents the location of the center of the j-th platform joint with respect to the center of gravity of the

platform plate. Note that $\boldsymbol{l}_j$ and $\boldsymbol{B}_j$ are dependent on the tool position and orientation, $\boldsymbol{T}$. The symbol $\times$ denotes the outer product of two vectors. Notice that when x_j represents an axial force on the j-th strut, the first three components of the vector $\Gamma_{l,B}(x)$ define the combined force vector of the axial forces. The last three components define the combined moment around the center of gravity of the platform plate imposed by the axial forces acting on platform joints.

The gravity imposed on the j-th platform joint in the direction of the j-th strut, $\hat{\boldsymbol{g}}=\{\hat{g}_j\}_{j=1\sim6}$, is given by solving the following equilibrium equation of force and moment around the center of gravity of the platform plate:

$$\Gamma_{l,B}(\hat{\boldsymbol{g}}-\boldsymbol{g}_s)=\begin{bmatrix}-\boldsymbol{N}_g\\-\boldsymbol{M}_g\end{bmatrix} \tag{4}$$

where $\boldsymbol{N}_g\in\boldsymbol{R}^3$ and $\boldsymbol{M}_g\in\boldsymbol{R}^3$ respectively represent an equivalent force and moment around the center of gravity of the platform plate given by the gravity acting on each strut. They are given as follows.

Figure 3 illustrates a gravity model for each strut. In the figure, m_P, m_B, m_J, and m_S represent the mass (in kg) of the platform plate, the ball screw, the platform joint, and the servo motor, respectively. l_1 is the distance (in meters) between the rotation center of a base joint and the center of gravity of a servo motor, l_2 is the length of the platform joint unit on a strut (in meters), and l_3 is the length of the ball screw (distance between the rotation center of a base joint and a platform joint) (in meters), and L_j is the total length of the j-th strut (in meters). By using this model, $\boldsymbol{N}_g$ and $\boldsymbol{M}_g$ are given as follows:

$$\boldsymbol{N}_g=m_P\boldsymbol{g}+\sum_{j=1}^{6}\boldsymbol{N}_{g,j},\quad \boldsymbol{M}_g=\sum_{j=1}^{6}\boldsymbol{M}_{g,j} \tag{5}$$

where $\boldsymbol{g}\in\boldsymbol{R}^3$ is a vector that represents the direction and the magnitude of the gravity. On each strut, the superposition of the gravity acting on a ball screw, a platform joint, and a servo motor can be represented as an equivalent moment around the rotation center of a base joint (see Fig. 3). On the j-th strut, this moment imposes an equivalent force, $\boldsymbol{N}_{g,j}$ in Eq. (5), at the center of the j-th platform joint in the direction perpendicular to the strut. Similarly, $\boldsymbol{M}_{g,j}\in\boldsymbol{R}^3$ represents an equivalent moment around the center of gravity of the platform plate imposed by $\boldsymbol{N}_{g,j}$ on the j-th strut. That is,

$$\boldsymbol{N}=\left[\frac{m_B\left(L_j-l_2-\frac{l_3}{2}\right)+m_JL_j-m_Sl_1}{L_j}\right]\boldsymbol{g}-\left\{\left[\frac{m_B\left(L_j-l_2-\frac{l_3}{2}\right)+m_JL_j-m_Sl_1}{L_j}\right]\boldsymbol{g}\cdot\boldsymbol{l}_j\right\}\boldsymbol{l}_j$$

$$\boldsymbol{M}=\boldsymbol{B}_j\times\left[\frac{m_B\left(L_j-l_2-\frac{l_3}{2}\right)+m_JL_j-m_Sl_1}{L_j}\right]\boldsymbol{g}-\boldsymbol{B}_j\times\left\{\left[\frac{m_B\left(L_j-l_2-\frac{l_3}{2}\right)+m_JL_j-m_Sl_1}{L_j}\right]\boldsymbol{g}\cdot\boldsymbol{l}_j\right\}\boldsymbol{l}_j \tag{6}$$

where the symbol $\cdot$ denotes the inner product of two vectors. In Eq. (4), the j-th component of the vector $\boldsymbol{g}_s\in\boldsymbol{R}^6$ represents the axial component of the gravity acting on the j-th strut. It is given by:

$$\{\boldsymbol{g}_s\}_j=m_j\boldsymbol{g}\cdot\boldsymbol{l}_j \tag{7}$$

where m_j represents the total mass of the j-th strut.

3.1.2 Friction model for each strut On each strut, we consider: 1) linear friction on a ball screw, and 2) angular friction in a base joint. The total friction force in the direction of the j-th strut, $\hat{\boldsymbol{f}}=\{\hat{f}_j\}_{1\sim6}$, is given by solving the following equation:

$$\Gamma_{l,B}(\hat{\boldsymbol{f}}-\boldsymbol{f}_b)=\begin{bmatrix}-\boldsymbol{N}_c\\-\boldsymbol{M}_c\end{bmatrix} \tag{8}$$

where $\boldsymbol{f}_b\in\boldsymbol{R}^6$ represents linear friction (in N) between a ball screw and a nut, and is given by the following simple model:

$$\{\boldsymbol{f}_b\}_j=\begin{cases}-f_{0j} & (\dot{L}_j>0)\\ +f_{0j} & (\dot{L}_j<0)\end{cases} \tag{9}$$

where f_{0j} is constant. $\dot{L}_j$ represents the axial velocity of the j-th strut. f_{0j} may depend on the velocity or the direction of the strut. In our experimental machine, however, such an effect was sufficiently small and thus is neglected for simplicity of the model.

In Eq. (8), $\boldsymbol{N}_c$, and $\boldsymbol{M}_c\in\boldsymbol{R}^3$ respectively represent an equivalent force and moment around the center of gravity of the platform plate given by an angular friction in each base joint. As illustrated in Fig. 4, angular friction in a base joint is modeled as an equivalent force acting on the platform joint in the direction perpendicular to the strut. $\boldsymbol{N}_c$ represents the superposition of such forces, and $\boldsymbol{M}_c$ represents the superposition of moments around the center of gravity of the platform plate imposed by such forces. That is,

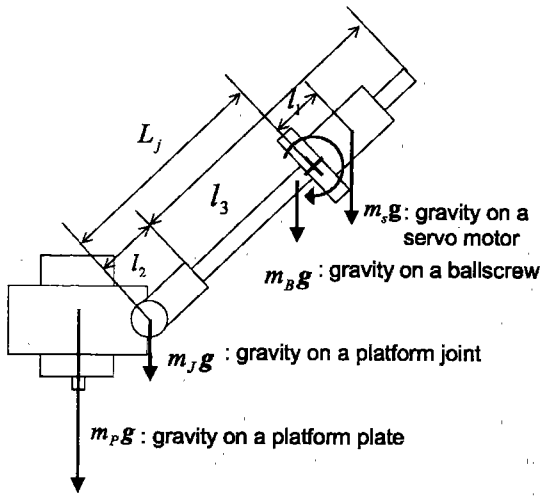

Fig. 3 A gravity model on a strut

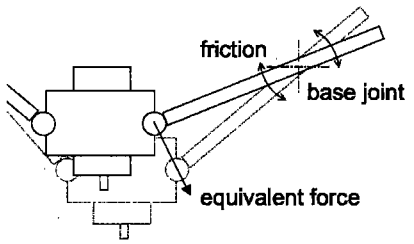

Fig. 4 The friction on a base joint

$$N_c = -\sum_{j=1}^{6} \frac{c\omega_j}{\zeta}$$
$$M_c = -\sum_{j=1}^{6} B_j \times \frac{c\omega_j}{\zeta} \quad (10)$$

where $c \in R$ is the angular viscous friction coefficient in a base joint (in Ns/m). For simplicity of the model, c is assumed constant for all the base joints. $\zeta \in R$ represents the feed rate of the spindle unit (in m/s), and $\omega_j \in R^3$ represents an angular velocity vector (in rad/s) of the j-th strut with respect to the center of the j-th base joint.

3.1.3 Estimation of positioning error To summarize the discussion above, when the position and the orientation of the tool tip, T, are given, the axial force on each strut can be estimated as follows: 1) for given T, compute the orientation of struts, l, and the position of platform joints with respect to the center of gravity of the platform plate, B, by solving the inverse kinematics problem. 2) Calculate $\hat{g}$ and $\hat{f}$ by algebraically solving Eqs. (4) and (8), respectively. 3) The estimated axial force on each strut, $\hat{F} \in R^6$, is given by $\hat{F} = \hat{g} + \hat{f}$.

The elastic deformation of the j-th strut in the axial direction is assumed to be simply proportional to $\{\hat{F}\}_j$. That is, the axial deformation of the j-th strut, $\{\Delta\hat{L}\}_j$, is given by:

$$\{\Delta\hat{L}\}_j = \{K_{\text{stiff}}\}_j \{\hat{F}\}_j \quad (11)$$

where $\{K_{\text{stiff}}\}_j$ ($j=1-6$) represents the axial compliance of the j-th strut (in m/N). It is modeled as:

$$\{K_{\text{stiff}}\}_j = K_1 L_j + K_2 \quad (12)$$

where K_1, $K_2 \in R$ are constant for all the strut. As will be presented in section 3.2, these parameters must be identified based on actual measurement of the machine's contouring error.

The resultant positioning error at the tool tip, $\Delta\hat{T} \in R^6$, is given as the superposition of the deformation of each strut. That is,

$$\Delta\hat{T} = \mathcal{F}^{-1}(\hat{L} + \Delta\hat{L}) - \hat{T} \quad (13)$$

where $\hat{T} \in R^6$ represents the commanded position and orientation of the tool tip. $\hat{L} \in R^6$ represents the reference length of struts given by $\hat{L} = \mathcal{F}(\hat{T})$.

3.2 Identification of model parameters

The present estimation model is simple, and the parameters included in the model can be identified by simple tests to measure the machine's dynamics and contouring performance. To improve the estimation accuracy, some of the parameters included in the estimation model must be experimentally identified as follows.

The parameters, m_s in Eq. (6), m_j in Eq. (7), f_b in Eq. (9), and c in Eq. (10), can be identified by monitoring the armature current in servo motors in a circular operation. In our experimentation, these parameters were identified based on circular tests

Table 2 Conditions of circular tests for the identification of model parameters

Name	Center location, mm			Radius,	Tilt angle, deg	
	X	Y	Z	mm	A	B
A	0	100	-1008	144	0	0
B	0	100	-1008	144	-23	0

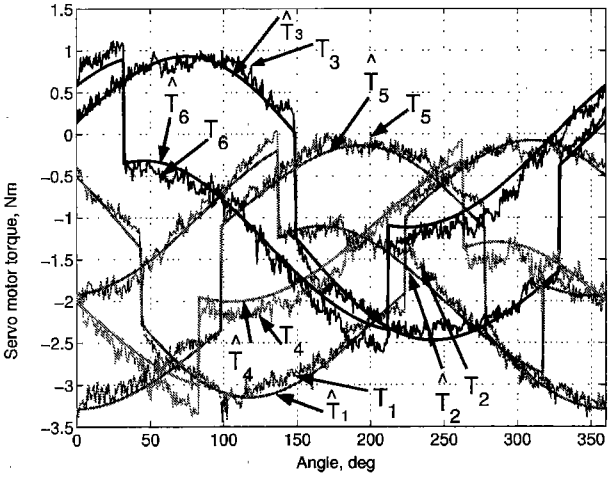

(a) Condition A

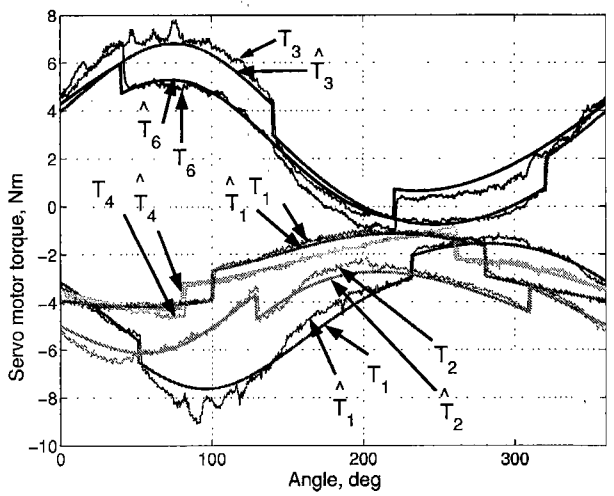

(b) Condition B

Fig. 5 Comparison of measured (T_i) and simulated ($\hat{T}_i$) servo motor torque profiles on each strut ($i=1-6$) in a circular operation

conducted under two conditions as shown in Table 2. Figure 5(a) and (b) show servo motor torque profiles (T_1 - T_6) in a circular operation under these two conditions. In both tests, the feed rate was 1 000 mm/min, the reference trajectory radius was 144 mm, and the orientation was CCW (counter clockwise). The figures also show the estimates of servo motor torque ($\hat{T}_1$ - $\hat{T}_1$) by the present model with the identified parameters.

It can be observed that unlike serial kinematic feed drives, servo motor loads in a parallel kinematic feed drive markedly vary as the position and orientation of the spindle change. The model parameters are identified such that the error between measured and estimated motor load profiles is minimized. The mean of the error between measured and estimated profiles is 0.11 Nm in the condition A, and 0.25 Nm in the condition B.

The parameters, K_1 and K_2 in Eq.(12), can be identified based on the measurement of the machine's contouring error in a circular operation. Contouring error profiles are measured by the DBB test (see section 4) in the conditions A and B given in Table 2. K_1 and K_2 are identified such that the error between measured and simulated contouring error profiles is minimized. The identified parameters are: m_S=22 (kg), m_J=250 (N), $c=3.5\times10^{-5}$ (Ns/m), $\boldsymbol{f}_b$={110, 130, 160, 130, 160, 160} (N), $K_1=1.287\times10^{-11}$ (m/N), and $K_2=7.82\times10^{-9}$ (m/N).

3.3 Compensation of reference trajectory

When a positioning error at the tool tip is estimated by using the present simulator, it can be compensated by simply shifting the command position. For the given command position (and orientation), $\hat{\boldsymbol{T}}$, suppose that the estimated error is given by $\Delta\hat{\boldsymbol{T}}$. Then, the command position must be shifted to $\hat{\boldsymbol{T}}_{\text{comp}} := \hat{\boldsymbol{T}} - \Delta\hat{\boldsymbol{T}}$ to cancel the estimated positioning error.

4. Experimental Validation

The validity of the present compensation method of gravity-induced motion errors was experimentally verified for the Hexapod-type parallel kinematic machine tool described in section 2.1. The machine's contouring accuracy was measured by circular tests using the DBB (double ball bar) device shown in Fig. 6. The distance between the ball A, which is attached to the spindle, and the ball B, which is fixed on the table, is measured by an encoder installed in the bar. The machine's contouring error is measured as the spindle moves along a circular path centering the location of the fixed ball[12].

First, the estimation performance of the proposed model was tested. As examples, Fig. 7(a) and (b)

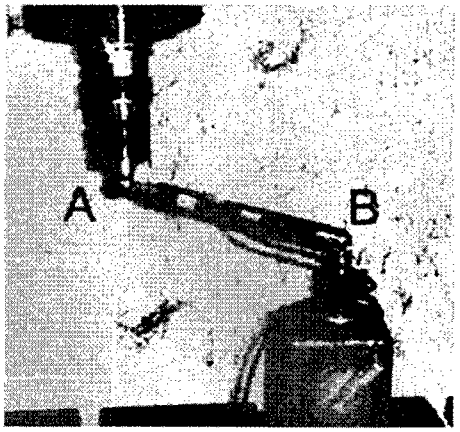

Fig. 6 A DBB device

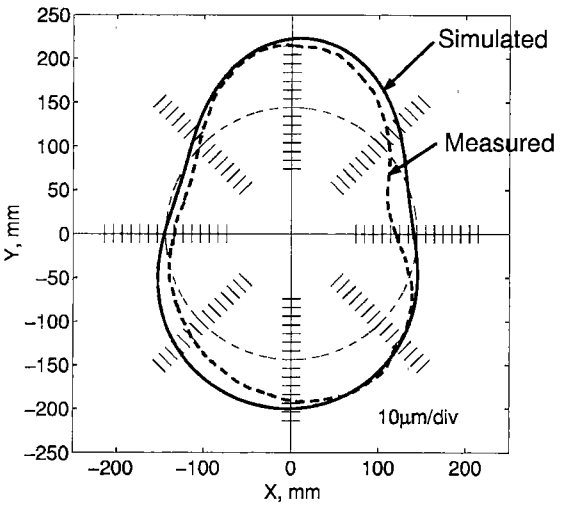

(a) Center location $(X, Y, Z)=(0, 100, -1\,008)$ (mm), tilt angle $(A, B)=(-23, 0)$ (deg)

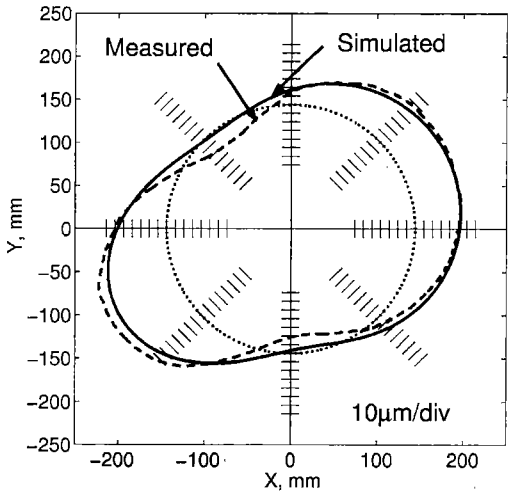

(b) Center location $(X, Y, Z)=(-70, -70, -1\,008)$ (mm), tilt angle $(A, B)=(-17, -17)$ (deg)

Fig. 7 Comparison of measured (dashed line) and simulated (solid line) contouring error profiles in a circular operation

show the comparison of measured and estimated contouring error profiles in a circular operation at different locations (Fig. 7(a) : center location (X, Y, Z)=(0, 100, −1 008) (mm), tilt angle (A, B)=(−23, 0) (deg), Fig. 7(b) : center location (X, Y, Z)=(−70, −70, −1 008) (mm), tilt angle (A, B)=(−17, −17) (deg)). In both tests, the feed rate was 1 000 mm/min, the reference trajectory radius was 144 mm, and the rotation direction was CCW. Notice that the contouring error trajectory in (a) was used in the model identification (see section 3.2), while the error trajectory in (b) was not. The figures show good agreement between simulated and measured profiles in both cases.

Then, the compensation performance of the proposed scheme for such a gravity-induced motion error was tested. At every 0.1° from the starting point on a circular path, the positioning error is estimated and then the reference point is shifted to cancel it. Circular tests were conducted with the same center location of (X, Y, Z)=(0, 100, −1 008) mm and various tilt angles, A=−25, −23, −20, −10, 0, +10, +20 deg (B=0 deg in all the tests). Other conditions in the circular tests were the same as in the previous tests.

Figure 8 summarizes the circularity error with and without the compensation in each test. Without the compensation, the circularity error drastically increases as the tilt angle increases in the negative direction. The proposed compensation method significantly reduces the circularity error particularly under such a condition. For example, when the tilt angle A was −25 deg, the circularity error without the compensation was as large as 200.6 μm. By applying the compensation, it was reduced to 44.5 μm (77.9% reduction). When the tilt angle is smaller, the circularity error is originally much smaller without the compensation (when the tilt angle is $-10 \leq A \leq 20$ deg, the circularity error is less than 15 μm). Even in such a case, where the gravity does not impose much effect on the machine's positioning accuracy, the proposed compensation scheme can further reduce the circularity error slightly.

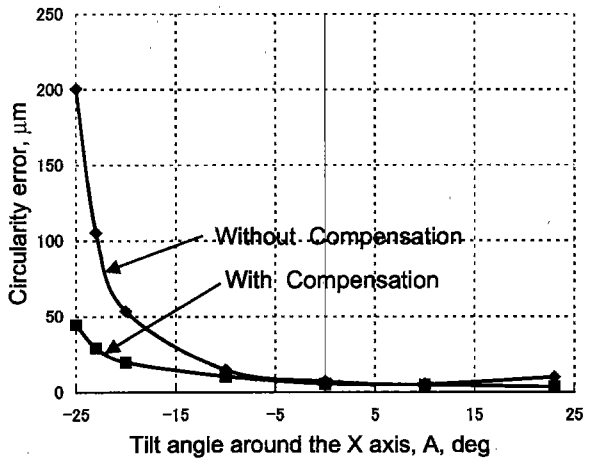

Fig. 8 Comparison of the circularity error with and without the compensation (center location: (X, Y, Z)=(0, 100, −1 008) mm, tilt angle: B=0 deg, A=−25 - +20 deg)

Figure 9(a) shows the comparison of measured contouring error profiles with and without the compensation when the tilt angle is A=−25 deg. As another example, Fig. 9(b) shows contouring error profiles with the center location of (X, Y, Z)=(−70, −70, −1 008) mm and the tilt angle of (A, B)=(−17,

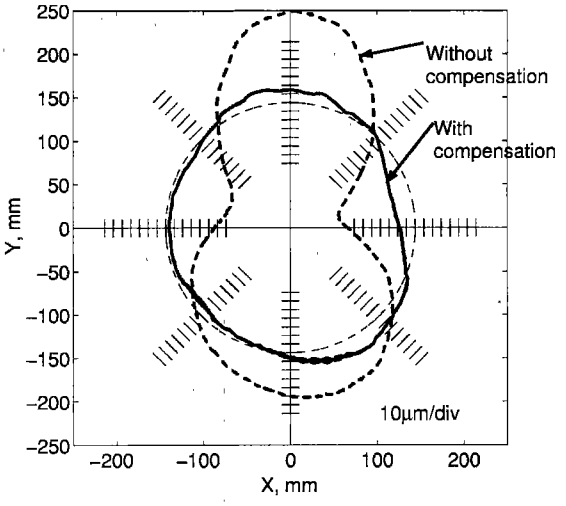

(a) Center location (X, Y, Z)=(0, 100, −1 008) (mm), tilt angle (A, B)=(−25, 0) (deg)

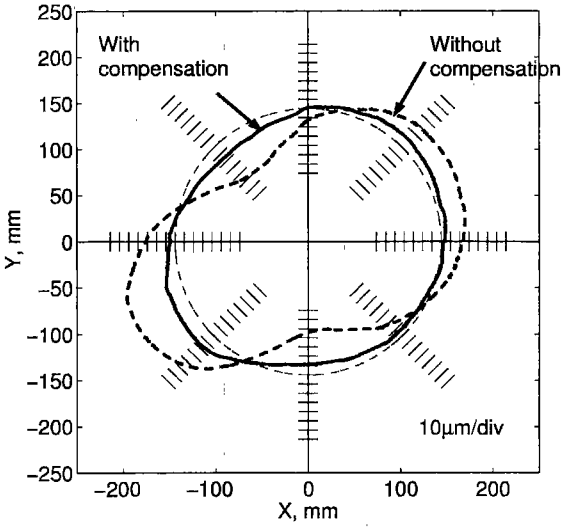

(b) Center location (X, Y, Z)=(−70, −70, −1 008) (mm), tilt angle (A, B)=(−17, −17) (deg)

Fig. 9 Comparison of contouring error profiles in a circular operation with (solid line) and without (dashed line) the compensation

−17) deg. In this case, the circularity error was reduced from 116.2 μm to 35.6 μm (69.4% reduction) by applying the compensation.

5. Conclusion

This paper presented a compensation scheme of contouring errors introduced by gravity for a Hexapod-type parallel kinematic machine tool. The following conclusions are drawn:

1. A simulator to predict gravity-induced errors was proposed. The simulation parameters are identified based on measured contouring error profiles and servo motor current profiles in circular tests. Simulated contouring error profiles showed good agreement with measured ones.

2. By compensating a reference trajectory based on the estimate of the positioning error, the machine's contouring performance can be significantly improved particularly when the machine is near a singular point in its workspace. When the tilt angle of the spindle around the X-axis was more than 20 degrees, the circularity error was reduced by about 80% at maximum.

Finally, it should be emphasized that accurate calibration of kinematic parameters is crucial for an effective compensation of gravity-induced positioning errors. If the positioning error due to the miscalibration of kinematic parameters is large, it is difficult to distinguish the positioning error caused by the gravity. In other words, it becomes more difficult to simulate contouring errors by the proposed simulator. As has been briefly presented in section 1, we have proposed a kinematic calibration scheme in our previous works. Kinematic parameters used in the experiments were tuned such that they showed the best contouring performance to date. It may, however, still contain calibration errors to some extent. If the calibration error is further reduced, then further improvement by the gravity compensation is expected.

Acknowledgement

This work was supported in part by the JSPS Grants-in-Aid for Scientific Research (# 15560094).

References

(1) Weck, M. and Staimer, D., Parallel Kinematic Machine Tools—Current State and Future Potentials, Annals of the CIRP, Vol. 51, No. 2 (2002), pp. 671-683.

(2) Weck, M. and Staimer, D., Accuracy Issues of Parallel Kinematic Machine Tools, Compensation and Calibration, Proc. of 2000 Parallel Kinematic Machines Int. Conf., (2000), pp. 35-41.

(3) Soons, J.A., Measuring the Geometric Errors of a Hexapod Machine Tool, Laser Metrology and Machine Performance IV, (1999), pp. 169-182, WIT Press.

(4) ISO 230-4, Test Code for Machine Tools—Part 4: Circular Tests for Numerically Controlled Machine Tools, (1996).

(5) Ota, H., Shibukawa, T., Tooyama, T. and Uchiyama, M., Study of Kinematic Calibration Method for Parallel Mechanism (2nd Report)—Kinematic Calibration Using Forward Kinematics—, J. of Jpn. Soc. Prec. Eng., (in Japanese), Vol. 66, No. 10 (2000), pp. 1568-1572.

(6) Oiwa, T. and Kataoka, Y., A Calibration Method for Coordinate Measuring Machine Using Parallel Mechanism—Calibration with Double Ball Bar and Touch Trigger Probe—, J. of Jpn. Soc. Prec. Eng., (in Japanese), Vol. 69, No. 2 (2003), pp. 222-226.

(7) Takeda, Y., Shen, G. and Funabashi, H., Kinematic Calibration of In-Parallel Actuated Mechanisms Using Fourier Series (1st Report, Calibration Method and Selection Method of the Set of Measurement Paths), Trans. of Jpn. Soc. Mech. Eng. Series C, (in Japanese), Vol. 68, No. 673 (2002), pp. 2762-2769.

(8) Nakagawa, M., Matsushita, T., Watanabe, S., Kakino, Y. and Ihara, Y., The Improvement of Motion Accuracy of Hexapod-Type Machine Tools and Its Machining Performance, Proc. of 2002 Japan-USA Symp. on Flexible Automation, Vol. 2 (2002), pp. 979-982.

(9) Ota, H., Shibukawa, T., Tooyama, T. and Uchiyama, M., Study of Kinematic Calibration Method for Parallel Mechanism (3rd Report)—Gravity Compensation and Kinematic Calibration Considering Gravity—, J. of Jpn. Soc. Prec. Eng., (in Japanese), Vol. 66, No. 10 (2000), pp. 1568-1572.

(10) Stewart, D., A Platform with Six Degrees of Freedom, Proc. of the Inst. of Mech. Eng., Vol. 180, Part 1, No. 15 (1965), pp. 371-386.

(11) Takaoka, H., Kakino, Y., Ibaraki, S., Nakagawa, M., Matsushita, T. and Jintsu, K., Compensation of Motion Errors Due to the Gravity for Parallel-Link Machine Tools, Proc. of the 2002 Fall JSPE Conf., (in Japanese), (2002), p. 236.

(12) Kakino, Y., Ihara, Y. and Shinohara, A., Accuracy Inspection of NC Machine Tools by Double Ball Bar Method, (1993), Carl Hanser Verlag.